A Path to High Efficiency Optical Coupling for HIRMES

Timothy M. Miller[1] • Ari-David Brown[1] • Nicholas Costen[1, 2] • David Franz[1] • Alexander Kutyrev[1, 3] • Vilem Mikula[1, 4] • Kevin H. Miller[1] • S. Harvey Moseley[1] • Joseph Oxborrow[5] • Karwan Rostem[1, 3] • Edward J. Wollack[1]

1. *NASA Goddard Space Flight Center, 8800 Greenbelt Rd, Greenbelt, MD 20771 USA*
2. *Stinger Ghaffarian Technologies, 7515 Mission Drive, Suite 300, Seabrook, MD 20706 USA*
3. *Department of Astronomy, University of Maryland, College Park, MD 20742 USA*
4. *Institute for Astrophysics and Computational Science, Catholic University of America, 620 Michigan Ave N.E., Washington, DC 20064 USA*
5. *Scientific and Biomedical Microsystems, 806 Cromwell Park Drive Suite R, Glen Burnie, MD 21061 USA*

Abstract The high-resolution mid-infrared spectrometer (HIRMES) under development for SOFIA (Stratospheric Observatory for Infrared Astronomy) is an instrument operating in the 25-122 μm spectral range with a spectral resolution $R=\Delta\lambda/\lambda\sim100{,}000$ and has two absorber-coupled transition edge sensor (TES) bolometric detector focal planes. We have developed novel NbTiN low stress absorber coatings which have the required optical impedance across the HIRMES operating band. The low intrinsic stress of these coatings allow for a peak-to-valley corrugation amplitude < 5 μm of the 450 nm thick, 1.4 mm x 1.7 mm detector pixels. Furthermore, these coatings have a superconducting transition temperature ~ 10 K, which allows them to simultaneously serve as an absorber in the desired signal band and a rejection filter at long wavelengths. This attribute makes them especially attractive for ultrasensitive absorber-coupled bolometric detector applications, because it helps in controlling the optical loading from out-of-band radiation. We also discuss a novel method for integrating a wedged-reflective absorber-termination to the detector array.

Keywords Transition edge sensor • HIRMES • Bolometer • Optical Coupling

1 Introduction

Timothy M. Miller • Ari-David Brown • Nicholas Costen • David Franz • Alexander Kutyrev • Vilem Mikula • Kevin H. Miller • S. Harvey Moseley • Joseph Oxborrow • Karwan Rostem • Edward J. Wollack

The HIRMES instrument is a high resolving power mid-infrared (25-122 μm) spectrometer that is planned to fly on the airborne Stratospheric Observatory for Infrared Astronomy (SOFIA) in 2019 [1]. HIRMES will have two bolometric detector arrays for its two spectral resolving modes: A high-resolution, narrow bandwidth – within each of its 1x16 detector sub-arrays – background-limited detector array, and a low-resolution broadband detector array [2].

We have fabricated the 64x16 low-resolution and 8x16 high-resolution detector arrays for the HIRMES instrument. Both the high and low-resolution detectors consist of Mo/Au bilayer thin film TES deposited on leg-isolated single crystal silicon membranes that were 0.45 μm and 1.40 μm thick, respectively. The low-resolution detector pixels have a uniform 1 mm square geometry, whereas the size of the high-resolution detector pixels in each row is designed to optimize the coupling to HIRMES' point spread function and ranges between 0.4 and 1.4 mm. The detector pixels on one camera, the high-resolution detector array, will be optically coupled to a quarter-wave backshort. Consequently, in order to achieve high optical efficiency, the absorber-coupled detector pixels need to be flat to within ~λ/10. More details on the fabrication of these arrays are presented in these proceedings [2].

The optical coupling scheme varies greatly for both the low- and high-resolution arrays. In the case of the low-resolution array, a frequency independent absorber architecture can be employed in a manner previously demonstrated on other instruments [3, 4, 5]. For the high-resolution array, due to the range in pixel size, a more complicated scheme was developed. In this proceeding, we describe the optical coupling plan and associated fabrication and assembly processes required to realize the two types of HIRMES detector arrays.

2 Absorber Coatings

The absorber material chosen for the high-resolution design is NbTiN, which is sputter deposited onto the backside of each pixel using a co-deposition process in a nitrogen background and is done at the chip level. We have developed a material with intrinsic film stress on a silicon substrate less than 200 MPa, superconducting transition temperature ~10K, and resistivity ~3000 μΩ cm. The first attribute allows for minimal peak-to-valley corrugation of the Si membranes (< 5 μm for a 1.4 mm pixel), the

second allows for >96% rejection of 4.2K thermal radiation, and the third allows for ease of fabrication, because the timescales required to deposit a film with the optical surface impedance of 200-500 Ω/square are readily accessible and reproducible.

This material is also stable at room temperature for long durations as shown in Fig. 1. Post deposition, a representative film was stored in a continually purged dry nitrogen box until ready for measurement. The sheet resistance shows an initial period of increase but becomes stable over long periods of time within a usable range for HIRMES.

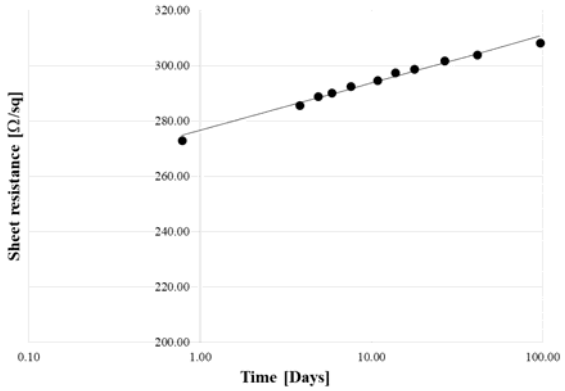

Fig. 1 Semi-log plot showing aging data for a NbTiN film (dots). The line is a linear fit with functional form $R_s = a \log_{10}(t) + b$, where a = 17.177 and b = 276.47.

The absorber material chosen for the low-resolution design is Mo_2N. This material sheet resistance has been proven to be weakly susceptible to aging, as shown in Fig. 2, and can be easily reproduced. Transmittance data over twice the HIRMES working band was obtained using a Bruker IFS125 HR Fourier transform spectrometer (FTS) at 300K and 10K. The film is deposited by sputtering onto the backside of each pixel in a nitrogen background and is done at the chip level. The parameters for the as-deposited film are thickness~14 nm, sheet resistance ~140 Ω/square, and residual resistance ratio ~0.9 to achieve a frequency-independent absorber coating on a silicon membrane at cryogenic temperature. Fits to the data in Fig. 2 using a transmission line model give an estimated optical impedance of ~140 Ω/square at 300 K and ~160 Ω/square at 10K, which enables a broadband optical efficiency ~ 0.45.

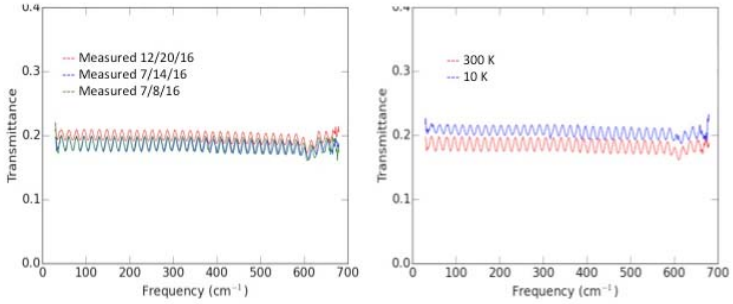

Fig. 2 Transmittance data of the Mo_2N absorber coating for the low-resolution HIRMES array. Extracted values of the optical impedance of the FTS data taken five months apart (left) show the vary by less than 10%. Also shown (right) is FTS data of the coating at 10 and 300 K.

3 Gap-Controlled Optical Coupling

For radiation that is transmitted through the impedance-matched absorbers on the high- and low-resolution arrays there is either a resonant reflective or absorptive termination structure, respectively. A cross-section at the pixel scale of the optical coupling design for each array is depicted in Fig. 3.

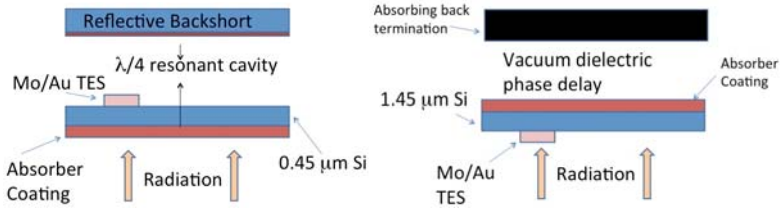

Fig. 3 A pixel scale representation of the optical coupling scheme for the high- (left) and low- (right) resolution arrays for HIRMES.

For the low-resolution array, the pixel dimension is uniform, requiring frequency independent coupling across the entire 25-122 μm spectral band. Consequently, the coupling design is relatively straightforward and optimal coating impedance is determined by the index of refraction of the substrate [6, 7]. As mentioned above, the high-resolution array has a different size pixel for each row, with each row targeting a different waveband – thus a

wedged backshort is required to achieve high optical coupling at each waveband as depicted in Fig. 4. A quarter-wave resonant cavity at each row with a wedged design presents some assembly difficulties in the limit of small gap spacing, thus cleanliness and alignment are critical.

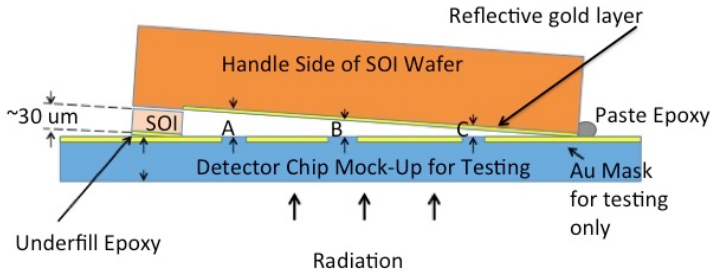

Fig. 4 Wedged backshort design for the high-resolution array for HIRMES. Depicted is a model of a mock assembly scheme which allowed for assembling and testing parts to verify the gaps required at positions labeled A, B and C.

Whereas the assembly and execution of a wedged backshort is difficult, the fabrication is straightforward. Using a silicon-on-insulator (SOI) wafer, one can set the angle of the wedge by selecting the SOI thickness for a given backshort dimension. Backshort singulation is accomplished using the Bosch deep etching technique around the perimeter. Prior to singulation, the silicon device and buried oxide layers are etched away leaving behind a step on one side of the chip. Finally, the etched surface is coated with gold to present a reflecting surface to the incoming radiation.

The assembly of the backshort and array is done at the chip level. Extensive inspection and cleaning is done on both parts to ensure no particle interferes in the gap. The backshort is placed on the array using a Finetech Fineplacer pico-ma, which allows for alignment, placement and force control. Epoxies are placed with a single-hair brush while force is applied throughout the cure cycle.

Sample hybrids created using mockup parts demonstrated the process as being repeatable by consistently meeting the desired gap dimensions (to within 1 μm) at the specified locations as verified by measuring the cross-sections in a scanning electron microscope (SEM). Most importantly, using the SEM we can verify that one edge indeed has zero gap. Transferring the process to detector mechanical model arrays with full-size leg-isolated membrane pixels proved to be much more difficult. In our initial tests, the

smallest pixels became stuck to the reflective backshort which by design were intended to be located ~7-12 μm away [8]. We believe this is likely due to electrostatic, capillary, or Van der Waals forces acting to pull the membrane in contact with the backshort across the small gaps, often seen in MEMS devices [9, 10]. This effect was easily observed under a visual microscope. Bowing of the membranes with and without absorber was investigated with a Zygo NewView 7300 white light interferometer as a potential cause, and was deemed not to be the root cause as low curvature is seen in both cases.

In an effort to mitigate the capillary force we fabricated a new batch of backshort chips and applied an anti-stiction coating to the surface of the deposited gold layer using an Integrated Surface Technologies RPX-540 vapor deposition system. The coating used is perfluorodecyltrichlorosilane, also known as FDTS, a long chain that produces hydrophobic surfaces, which has been shown to prevent stiction in MEMS devices [11]. In addition, during all aspects of assembly we utilized ionizing fans. The fans were directed at both parts during cleaning, bringing of the parts together and throughout the cure cycle. Both of these efforts are shown to have greatly improved our results, shown in Table 1. Gap measurements were verified with a high power visible light microscope by looking through the membrane surface down to the backshort. This method allowed verification in multiple locations of each row of the high-resolution array. All locations measured the expected gap with no sign of contact between membrane and backshort.

Array Row	**1**	**2**	**3**	**4**	**5**	**6**	**7**	**8**
Expected Gap [μm]	7.5	9.0	10.7	12.8	15.3	18.4	21.9	26.3
Measured Gap [μm]	8.5	11.5	11.5	-	-	19.5	-	29.0

Table 1 Gap measurements of a high-resolution array hybridized to a wedged backshort taken at several row locations. The missing values in the table are due to broken pixels in those rows.

4 Conclusions

The Path to Achieving High Optical Coupling for HIRMES

We have developed novel impedance-matched absorber materials for the HIRMES detectors as well as a process for fabricating and hybridizing a reflective quarter-wave backshort. Due to the minimal fabrication complexity required to realize the backshort, we anticipate that its use will be widely implemented for future mid- to far-infrared astronomical applications employing cryogenic absorber-coupled detectors.

5 References

1. https://www.nasa.gov/feature/nasa-selects-next-generation-spectrometer-for-sofia-flying-observatory.
2. A.-D. Brown et al, J. Low Temp. Phys. **This Special Issue** (2017).
3. C. Allen, D. J. Benford, T. M. Miller, S. H. Moseley, J. G. Staguhn, E. J. Wollack, J. Low Temp. Phys. **151**, 266-270 (2008), DOI: 10.1007/s10909-007-9646-9.
4. C. A. Jhabvala, et al, SPIE Proc **9153**, 9153C1-C12 (2014), DOI: 10.1117/12.2056995.
5. D. J. Benford, D. T. Chuss, G. C. Hilton, K. D. Irwin, N. S. Jethava, C. A. Jhabvala, A. J. Kogut, T. M. Miller, P. Mirel, S. Harvey Moseley, K. Rostem, E. H. Sharp, J. G. Staguhn, G. M. Stiehl, G. M. Voellmer, and E. J. Wollack, "5,120 superconducting bolometers for the PIPER balloon-borne CMB polarization experiment," SPIE Proc. **7741**, 77411Q (2010).
6. B. Carli and D. Iorio-Fili, "Absorption of Composite Bolometer," J. Opt. Soc. of Am. **71**, 1020-1025 (1981).
7. The actual membrane-backshort separation distance may have been much shorter due to membrane curvature.
8. E. J. Wollack, D. T. Chuss, and S. H. Moseley, "Electromagnetic considerations for pixellated planar bolometer arrays in the single-mode limit," SPIE Proc. **6275**, 62750V (2006).
9. Z. Yapu, "Stiction and anti-stiction in MEMS and NEMS," Acta Mech. Sinica **19**, 1-10 (2003).
10. W. D. Greason, "Review of the Effect of ESD in MEMS," Proc. of the 2010 ESA Ann. Meeting on Electrostatics, June 22-24, 2010. University of North Carolina, Charlotte.
11. M. J. Li et al., "Electrostatic Microshutter Arrays", Transducers 2017 Conference, the 19th International Conference on Solid-State Sensors, Actuators and Microsystems, June 18-22, 2017. Kaohsiung, Taiwan.

Acknowledgements This work was supported by a SOFIA Third Generation Instrument Award. The authors gratefully acknowledge suggestions and discussions with Kevin Denis.